Optics Letters

Variation analysis of photonic lantern mode control ability under mode oscillation: a new approach

Xinrui Zhao,[1,2] Jie Liu,[1] Biao Wang,[1] Xihong Fu,[1] Yijia Dong,[1,2] Xingchen Lin,[1] Yongqiang Ning,[1] Lijun Wang,[1] and Hongbo Zhu[1,*]

[1]Changchun Institute of Optics, Fine Mechanics and Physics (CIOMP), Chinese Academy of Sciences, China
[2]University of Chinese Academy of Sciences, Beijing 100049, China
*zhbciomp@163.com

Received 21 April 2023; revised 14 May 2023; accepted 16 May 2023; posted 16 May 2023; published 2 June 2023

In this Letter, we present a novel, to the best of our knowledge, image-based approach to analyze the mode control ability of a photonic lantern employed in diode laser beam combining, aiming to achieve a stable beam output. The proposed method is founded on theories of power flow and mode coupling and is validated through experiments. The findings demonstrate that the analysis of the beam combining process is highly reliable when the main mode component of the output light is the fundamental mode. Moreover, it is experimentally demonstrated that the mode control performance of the photonic lantern significantly influences the beam combining loss and the fundamental mode purity. In the essence of the variation-based analysis, a key advantage of the proposed method is its applicability even in the situation of a poor combined beam stability. The experiment only requires the collection of the far-field light images of the photonic lantern to characterize the model control ability, achieving an accuracy greater than 98%.

https://doi.org/10.1364/OL.493251

The advancement of diode laser beam combining technology is driven by the need for stable, high-power fundamental mode diode lasers [1–6]. These lasers are essential for applications such as high-precision machining, long-distance optical fiber communication, and as a high-intensity laser source. Compared with other kW-level diode laser beam combining technologies [7,8], photonic lantern beam combining has a lower loss, simpler structural expansion, and easier mode control, making it one of the ideal devices for combining many laser beams [9]. In a conventional scheme, an active mode control system dynamically controls the photonic lantern's multi-channel input light to ensure coherent beam combining and obtain a 1.27-kW fundamental mode output. However, observations of on-axis voltage measurements indicate that the output light field is unstable and cannot avoid the effects of transverse mode oscillations caused by the accumulation of fiber thermal loads [10]. Moreover, the operation of these systems is independent of prior knowledge, resulting in insufficient analysis of the impact of optical fiber thermal effects. Consequently, to enhance beam quality for combined light affected by mode oscillation, it is imperative to investigate and measure the variations in mode control performance as a function of power.

The conventional method uses the beam quality factor M^2 to characterize the quality of the output combined beam [11], or uses the spatial light modulator (SLM) filtering technique to decompose the mode components of an unstable combined beam [12] to access the device mode control performance. However, we may obtain inaccurate or even invalid M^2 measurement results due to the influence of interference light in the fiber cladding or mode jump caused by transverse mode oscillation effects [13,14]. Although the SLM filtering technology provides accurate results, it has high requirements for optical path alignment, complicated equipment, and prior knowledge. For fiber combining, a simple approach is to use the fiber coupling coefficient to characterize its mode control performance. This method uses the numerical solution of the Gloge flow equation and the near-mode coupling equation to analyze and solve the modal change process of beam combining in optical fibers. The obtained fiber coupling coefficient characterizes the fiber's ability to control the input spatial light mode and convert it into a stable light field with a dominant fundamental mode. This study has been previously employed to analyze the W-shaped fiber, double-clad circular fiber, etc [15,16].

In this work, we use the gray matrix extraction method to numerically output the power distribution of the light field. By sampling the pixel's gray value in the central area of the two-dimensional (2D) color far-field light image, we calculate the variance of the gray matrix instead of the variance of the angular power distribution of the light field. This allows us to calculate the change rate and analyze the variation of the photonic lantern mode control performance caused by the changes of the beam combining power. This approach simplifies both the measurement process and requirements. Furthermore, the image-based calculation has lower beam stability requirements than the traditional experimental-based measurement. This method is suitable for accessing the photonic lantern mode control performance under most experimental conditions and is well suited for exploring the working effect of new mode control technology on the photosynthetic beam process under high power with strong mode oscillation effect. The advantages of using the gray matrix for the numerical processing of the light field power distribution include simple measurement apparatuses, low environmental

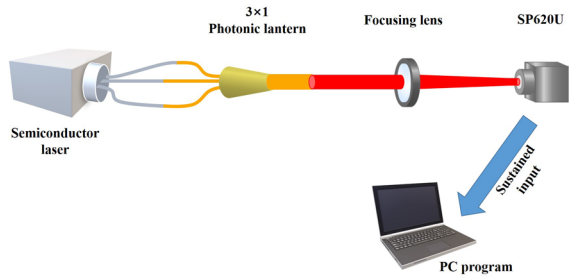

Fig. 1. Schematic of photonic lantern mode control performance variation analysis system.

requirement for measurement, fast processing speed, and avoidance of image analysis ambiguity, which is ideal for analyzing the output light field mode. For instance, a laser microscopic speckle analysis system can be constructed using the gray level co-occurrence matrix for speckle component evaluation in laser microscopy imaging [17].

Figure 1 shows the structure of the experimental device for analyzing the variation of the mode control performance of the photonic lantern. The distributed feedback diode laser is used to provide three fundamental mode diode lasers with the same power and polarization at the wavelength of 976 nm. The beams are combined by a 3×1 photonic lantern, and then focused by the lens to ensure that the light field is completely received by the CCD photosensitive chip. A CCD camera placed in front of the far-field focal plane receives 19 consecutive frames of far-field light field images at a given beam power. The CCD camera and software *BeamGage* are fixed accessories of the beam quality analyzer SP620U, which collect light field images and output 2D color images for data processing. In addition, the whole system uses a polarization-maintaining fiber to ensure the same optical polarization condition.

In our research, a photonic lantern with SMF-28 fiber input and two-mode graded-index SMF output is used. For the 976-nm laser transmission, the mode attenuation of fundamental and first-order modes is less than 0.22 dB/km, indicating that they are the primary modes supported in the fiber. Concurrently, higher-order modes are absorbed at the cone region of the fiber end. We use the power flow equation proposed by Gloge [18] and the adjacent mode coupling equation to analyze the light transmission process in the photonic lantern taper region, and characterize the performance of photonic lantern mode control based on the coupling coefficient developed by Savović [19]. The refractive-index difference between the core and cladding of the photonic lantern taper region fiber is 0.55%, allowing the discrete mode spectrum to be approximated as a modal continuum. A symmetrical arrangement of single-mode fibers is set up at the photonic lantern's input to ensure identical incident angle θ_i for input lights ($i=1, 2, 3$). Ignoring constant modal attenuation and conventional loss [20,21], the power flow equation in the taper region can be simplified as

$$\frac{\partial P(\theta,z)}{\partial z} = D\frac{\partial^2 P(\theta,z)}{\partial \theta^2}, \tag{1}$$

where z is the distance from the input to analyze location of taper fiber; $P(\theta,z)$ is the transverse power distribution as functions of incident angle and distance z. Solving $P(\theta,z)$ as a probability distribution function yields a proportional relationship between D and the rate of change of σ_z^2, that is, $D\propto\partial\sigma_z^2/\partial z$. The σ_z^2 is the variance of the far-field angular power distribution of the output light field.

For the beam with poor stability, the change of the far-field light distribution with the propagation distance includes two aspects: one is the increase of the light field area caused by the divergence angle of the output light, and the other is the influence of the mode oscillation on the shape of the light field. When we use the gray extraction algorithm to extract the power distribution of the entire light field, the influence of the divergence angle on the light field area can be directly avoided. As a result, the influence of the mode oscillation on the light field shape becomes the main measurement. Therefore, the measurement of the far-field angular power distribution variance with the transmission distance can be replaced by the change rate of the angular power distribution variance of the far-field light image taken by the CCD camera at a fixed position, which simplifies the measurement.

The control performance of the photonic lantern mode is simplified as the variance rate of the angular power distribution of the output far-field light distribution at a fixed position. The angular power distribution variance of the light field is typically used to describe the statistical characteristics of the light field in the spatial frequency domain, which can reflect the uniformity of the power distribution of the light field at different spatial frequencies. We use a new method to measure the variance of the angular power distribution, that is, recording multiple far-field images in a fixed period of time, extracting the gray matrix, and calculating the variance of the matrix value to characterize the variance of the angular power distribution. The formula of variance is shown by

$$g_i^2 = \Sigma_{k=0}^{L-1}(g_k-\bar{g})^2 H(g), \tag{2}$$

where g_i^2 is the gray value distribution variance, index $i=1, 2, \ldots, 19$ in this experiment; g_k is the gray value of each pixel point; $\bar{g}$ is the average gray value; $H(g)$ is probability of occurrence of gray value g in the matrix; L is the number of elements in the matrix, which is 727×727 in this experiment.

The image processing on the PC side is shown in Fig. 2. The 2D far-field light image with three-channel colors is cropped to a centered 727×727 pixel image. Sampling maintains background consistency while avoiding inaccuracy from the photosensitive chip's edge data. The three-channel data are read separately, assigning different weights for R, G, and B according to the YCbCr color space separation principle. This separates brightness and chroma, avoiding the influence of chroma Cb or Cr on characterizing the variance of diagonal power distribution. The gray value matrix is extracted from the gray image and used to calculate the distribution variance

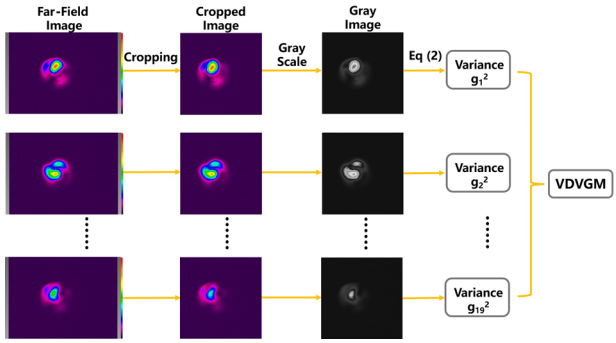

Fig. 2. Schematic of VDVGM calculation process.

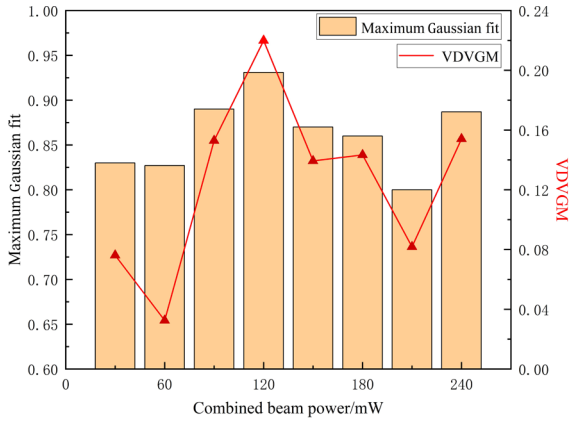

Fig. 3. Maximum Gaussian fit similarity and VDVGM as a function of combined beam power.

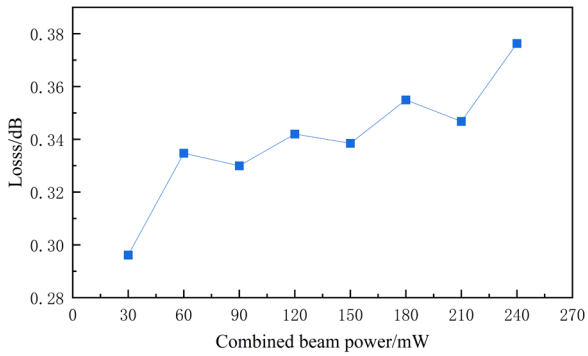

Fig. 4. Loss measurement of beam combining as a function of combined beam power.

instead of the brightness value. The distribution variance result not only characterizes the angular power distribution variance of each point in the light field, but the mode control performance of the photonic lantern. The single numerical result, rather than experimental measurements, simplifies the fluctuation analysis of the photonic lantern mode control performance. The variance of distribution variance of gray value matrix (VDVGM) of 19 gray distributions under a given beam combining power is calculated, followed by a normalization for performance comparison. In the obtained gray scale matrix, the brightness of the purple-black background area is uniformly identified as a matrix value ranging from 18 to 24, which is much lower than the value at the high-power region, avoiding background data interference.

We control the combined beam power between 30 and 240 mW in 30 mW increments to ensure that the main component of the combined beam is the fundamental mode, thus meeting the conditions for theoretical derivation. The change of the control performance of the photonic lantern mode in this range is analyzed. Figure 3 shows the maximum Gaussian fitting degree of the far-field light distribution recorded by the CCD and the corresponding VDVGM as a function of combined beam power. The Gaussian fitting degree is the similarity between the light power distribution and the normal distribution. The Gaussian fitting degrees of the standard LP_{01}, LP_{11o}, and LP_{11e} light fields generated by SP620U are 1, 0.55, and 0.526, respectively. The light field can be regarded as the superposition of multiple modes according to the respective power ratios. The maximum Gaussian fitting degree of the light field in the figure is between 0.75 and 1, which proves that the main mode component of the beam combining light is the fundamental mode.

As the combined beam power increases, the thermal effect of the fiber intensifies, and the mode oscillation becomes serious. However, the maximum Gaussian fitting degree of the output combined beam does not decrease with the increase of the combined beam power. When the combining power is less than 60 mW, the low power makes the thermal effect of the fiber very weak, and the maximum Gaussian fitting degree of the output light remains above 0.8. When the combined beam power increases from 60 mW to 120 mW, the VDVGM of the photonic lantern increases monotonically, implying the improvement of the mode control performance of the photonic lantern. This inhibits the energy transfer from the fundamental mode to the higher-order mode, thus ensuring the maximum Gaussian fitting degree that abnormally increases with the combined beam power, that is, the fundamental mode component ratio of the output light. The maximum point of VDVGM represents the best mode control performance of the photonic lantern cone structure in the detection range. When the mode control performance is good enough and the cone region is long enough, the photonic lantern can be tuned without any additional control. When the combined beam power ranges from 120 mW to 210 mW, we observed that the mode control ability of the photonic lantern decreases with the increase of the combined beam power, which leads to the decrease of the fundamental mode component ratio or the degradation of the Gaussian fitting degree. When the beam combining power reaches 210 mW or above, both the VDVGM and the fundamental model ratio increase, indicating an improved photonic lantern mode control ability of the photonic lantern.

We also measured the beam combining loss under different beam combining powers with a step size of 30 mW, as shown in Fig. 4. The strong mode control performance of the photonic lantern can suppress the energy transfer between the fundamental mode and the high-order mode, thereby reducing the loss of the combined beam when it enters the few-mode fiber from the end of the cone region. Near the beam combining power 60 mW that corresponds to the lowest mode control ability of the photonic lantern (see Fig. 3), we observed an abnormal beam combining loss maximum point (see Fig. 4), which is caused by the poor mode control ability of the photonic lantern. In contrast, as the combined power increases from 60 mW to 120 mW, a comparable loss is observed, which benefits from the good mode control ability. For the combined beam power in the range of 90–180 mW, the increased rate of the loss curve is significantly smaller than that in the range of 30–60 mW or 210–240 mW, proving the reliability of the VDVGM method in analyzing the change of photonic lantern and mode control ability.

The accuracy of performance evaluation is based on the accuracy of the brightness distribution representation of the light field based on the gray matrix. In the process of brightness reading, the calculation results are gray integers, which may introduce errors. As shown in Fig. 2, the background in the light field image may also introduce the palette color components unrelated to the coherent beam spot, potentially causing errors. We restore the color light field image based on the gray matrix, and perform histogram matching on the R, G, and B channels of the original image and the restored color light field image. The similarity calculation is shown as

$$\Delta S_x = \frac{\sum_{i=1}^{n} \min\left(H_{x1}(i), H_{x2}(i)\right)}{\min\left(\sum_{i=1}^{n} H_{x1}(i), \sum_{i=1}^{n} H_{x2}(i)\right)}, \tag{3}$$

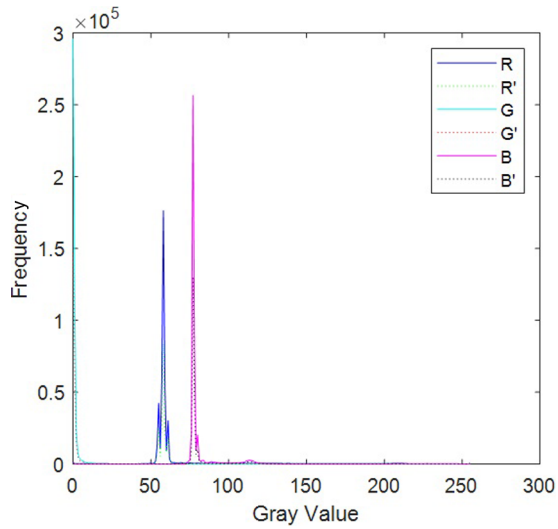

Fig. 5. Three-channel histogram comparison of the original diagram and the restored diagram. R, G, and B lines are for origin image, R', G', and B' lines are for restored colored light field image.

where $x = \mathrm{R}$, G, or B, ΔS_x is the result of x channel histogram similarity, $H_{x1}(i)$ is the histogram gray data of the original x channel, and $H_{x2}(i)$ is the histogram gray data of the x channel of the restored image. We then use the average value of the three-channel similarities as the final similarity metric. Figure 5 shows the histogram comparison of original and restored images with fundamental profile. The similarity between the two images is greater than 98%, proving that the numeric error induced by gray matrix extraction is less than 2%.

In summary, we demonstrate an analysis of the mode control performance of a 3×1 photonic lantern for the diode laser beam combining. Based on the theoretical derivation, we elucidate the working principle of the new scheme based on gray matrix extraction. When the combining power is approximately 60 mW, the low mode control performance of the photonic lantern leads to a local maximum of the combining loss. Conversely, when the beam power is approximately 120 mW, the stable trend in the beam loss, albeit with the increase of combined beam power, implies the improvement of the photonic lantern mode control performance and the suppression of the energy transfer between the fundamental and high-order modes. The image comparison indicates that the accuracy of the light field analysis is approximately 98%. The mode oscillation issue persists in the high-power beam combining of photonic lanterns, even equipped with external control systems. To address this, we have built an active mode control system to ensure that the main component of the combined high-power diode laser beam is the fundamental mode. In further work, we aim to utilize this characterization method to analyze the photonic lantern mode control performance to further optimize the active mode control algorithm or refine experimental parameters. Our method is based on the calculation of the output beam field variation, so it is still effective when the output field oscillates, which is very suitable for further improving the stability of the output field of the photonic lantern under active mode control. Ultimately, this will help to improve the transverse mode oscillation threshold of the diode laser beam combined photonic lantern.

Funding. National Natural Science Foundation of China (62222410, 62205336); Projects of Jilin Province Science and Technology Development Plan (20210201019GX).

Disclosures. The authors declare no conflicts of interest.

Data availability. Data underlying the results presented in this paper are not publicly available at this time but may be obtained from the authors upon reasonable request.

REFERENCES

1. X. Duan, J. Wu, R. Dou, Q. Zhang, T. Dai, and X. Yang, Opt. Express **29**, 12471 (2021).
2. B. Q. Yao, Y. J. Shen, X. M. Duan, T. Y. Dai, Y. L. Ju, and Y. Z. Wang, Opt. Lett. **39**, 6589 (2014).
3. H. Zhu, S. Fan, J. Zhao, X. Lin, L. Qin, and Y. Ning, IEEE Photonics J. **11**, 1502510 (2019).
4. X. Duan, C. Qian, Y. Shen, L. Su, L. Zheng, L. Li, B. Yao, and T. Dai, Opt. Express **27**, 4522 (2019).
5. Z. Zhou, Z. Wang, W. Huang, Y. Cui, H. Li, M. Wang, X. Xi, S. Gao, and Y. Wang, Light: Sci. Appl. **11**, 15 (2022).
6. S. Jin, R. Li, H. Huang, N. Jiang, J. Lin, S. Wang, Y. Zheng, X. Chen, and D. Chen, Light: Sci. Appl. **11**, 52 (2022).
7. M. Liu, W. Zhu, P. Huo, L. Feng, M. Song, C. Zhang, L. Chen, H. J. Lezec, Y. Lu, A. Agrawal, and T. Xu, Light: Sci. Appl. **10**, 107 (2021).
8. H. Zhu, X. Lin, Y. Zhang, J. Zhang, B. Wang, J. Zhang, L. Qin, Y. Ning, and H. Wu, Opt. Express **26**, 24723 (2018).
9. T. A. Birks, I. Gris-Sánchez, S. Yerolatsitis, S. G. Leon-Saval, and R. R. Thomson, Adv. Opt. Photonics **7**, 107 (2015).
10. C. Jauregui, C. Stihler, and J. Limpert, Adv. Opt. Photonics **12**, 429 (2020).
11. Y. Lu, Z. F. Jiang, W. G. Liu, Z. L. Chen, M. Jiang, Q. Zhou, and J. B. Zhang, Acta Opt. Sin. **41**, 239 (2021).
12. D. Flamm, C. Schulze, R. Brüning, O. A. Schmidt, T. Kaiser, S. Schröter, and M. Duparré, Appl. Opt. **51**, 987 (2012).
13. T. Eidam, C. Wirth, C. Jauregui, F. Stutzki, F. Jansen, H. J. Otto, O. Schmidt, T. Schreiber, J. Limpert, and A. Tünnermann, Opt. Express **19**, 13218 (2011).
14. X. Luo, P. Chen, and Y. Wang, Appl. Phys. B **98**, 181 (2010).
15. S. Savović, A. Djordjevich, A. Simović, and B. Drljača, Appl. Opt. **50**, 4170 (2011).
16. A. Simović, A. Djordjevich, and S. Savović, Appl. Opt. **51**, 4896 (2012).
17. Y. Liu, Q. Qin, H. H. Liu, Z. W. Tan, and M. G. Wang, Opt. Fiber Technol. **46**, 48 (2018).
18. D. Gloge, Bell Syst. Tech. J **51**, 1767 (1972).
19. S. Savović and A. Djordjevich, Appl. Opt. **47**, 4935 (2008).
20. S. Savović and A. Djordjevich, Laser Phys. **31**, 055102 (2021).
21. V. Ruddy and G. Shaw, Appl. Opt. **34**, 1003 (1995).